Point-cloud Mapping using Lidar Mounted on Two-wheeled Vehicle based on NDT Scan Matching

Kohei Tokorodani[1], Masafumi Hashimoto[2][a], Yusuke Aihara[1] and Kazuhiko Takahashi[2]

[1]Graduate School of Doshisha University, Kyotanabe, Kyoto 6100321, Japan
[2]Faculty of Science and Engineering, Doshisha University, Kyotanabe, Kyoto 6100321, Japan

Abstract: This paper presents a method for generating a 3D point-cloud map using multilayer lidar mounted on two-wheeled vehicle. The vehicle identifies its own 3D pose (position and attitude angle) in a lidar-scan period using the normal distributions transform (NDT) scan-matching method. The vehicle's pose is updated in a period shorter than the lidar-scan period using its attitude angle and angular velocity measured by an inertial measurement unit (IMU). The pose estimation is based on the extended Kalman filter (EKF) under the assumption that the vehicle moves at nearly constant translational and angular velocities. The vehicle's pose is further estimated in a period shorter than measurement period of the IMU using a linear interpolation method. The estimated poses of the vehicle are applied to distortion correction of lidar-scan data, and a point-cloud map is generated based on the corrected lidar-scan data. Experimental results of mapping a road environment using a 32-layer lidar mounted on a bicycle show the efficacy of the proposed method in comparison with conventional methods of distortion correction of lidar-scan data.

1   INTRODUCTION

In recent years, many studies have been conducted on the active safety and autonomous driving of vehicles and personal mobility devices. There are also many studies on last mile automation by delivery robots. Important technologies in these studies include the environmental map generation (Cadena et al., 2016) and map-matching based self-pose estimation by vehicles using the generated environment maps (Wang, et al., 2017).

In this study, we focus on map generation with a lidar mounted on a vehicle. In intelligent transportation systems (ITS) domains, maps are being generated using mobile mapping systems (Seif and Hu, 2016). Their maps are applied to autonomous driving and active safety for automobiles in wide road environments, such as highways, and major arterial roads. In this study, we consider environment maps for active safety and autonomous driving of personal mobility devices and delivery robots as well as for various social services such as disaster prevention and mitigation (Schwesinger et al., 2017, Morita et al., 2019).

To that end, we generate 3D point-cloud maps in narrow road environments, such as community roads and scenic roads in urban and mountainous areas, using lidar mounted on two-wheeled vehicles (bicycles and motorcycles) with higher maneuverability than four-wheeled vehicles. To generate 3D point-cloud maps using an onboard lidar, lidar-scan data captured in the sensor coordinate frame have to be accurately mapped on the world coordinate frame using pose (i.e., position and attitude angle) information of the vehicle. Since the lidar obtains scan data by laser scanning, all scan data within one scan cannot be obtained at the same time when a vehicle is moving or is changing its attitude. Therefore, if all scan data within one scan are transformed based on the vehicle's pose at the same time, distortion occurs in scan data mapped on the world coordinate frame.

To reduce distortion in the scan data, several methods have been proposed (Brenneke et al., 2003, Hong et al., 2010, Kawahara et al., 2006, Moosmann

---

[a] https://orcid.org/0000-0003-2274-2366

and Stiller, 2011, Zhang and Singh, 2014), in which the information of global navigation satellite system (GNSS), inertial measurement unit (IMU), or wheel encoder is observed within a short period, and the vehicle's pose is estimated in a period shorter than the lidar-scan period. In urban and mountainous environments, the GNSS information is often denied. Therefore, for the application in GNSS-denied environments, we proposed a method to correct distortion in the scan data using the normal distributions transform (NDT) scan matching and the extended Kalman filter (EKF) using only lidar information (Inui et al., 2017).

Most conventional methods were intended to correct distortion in lidar-scan data from a lidar mounted on four-wheeled vehicles, such as automobiles and mobile robots, moving on flat road surfaces. To the best of our knowledge, studies that have handled distortion correction when vehicles change their poses drastically are very few. Although several studies (Bosse et al., 2012, Kuramachi et al., 2015, Zhang and Singh, 2014) handled distortion correction in lidar-scan data from lidars with pose changes, their lidars were hand-held lidars which slowly change their poses.

Thus, in this paper, we propose a method that generates 3D point-cloud maps by correcting distortion in the scan data obtained from lidars mounted on two-wheeled vehicles that change their pose drastically, compared to lidars mounted on four-wheeled vehicles and hand-held lidars.

The rest of this paper is organized as follows. In Section 2, we give an overview of the experimental system. In Section 3, we summarize scan-data mapping based on the NDT scan matching. In Section 4, we present the distortion correction and mapping methods. In Section 5, we conduct experiments to reveal the performance of the proposed method, followed by conclusions in Section 6.

2 EXPERIMENTAL SYSTEM

Figure 1 shows the overview of the two-wheeled vehicle (YAMAHA electric bicycle). As the first step of the study, we use the bicycle as a two-wheeled vehicle.

On the upper part of the bicycle, a 32-layer lidar (Velodyne HDL-32E) and IMU (Tokyo Aircraft Instrument CSM-MG200) are mounted. The maximum range of the lidar is 70 m, the horizontal viewing angle is 360° with a resolution of 0.16°, and the vertical viewing angle is 41.34° with a resolution of 1.33°. The lidar provides 384 measurements (the
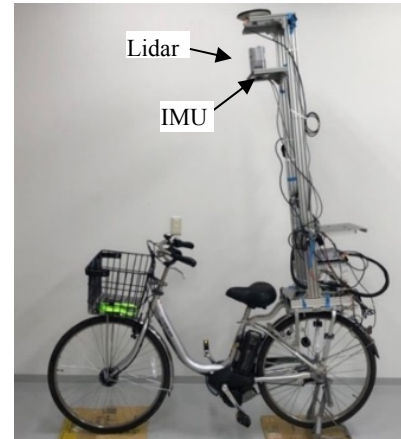
Figure 1: Overview of experimental bicycle.

object's 3D position and reflection intensity) every 0.55 ms (at 2° horizontal angle increments). The period for the lidar beam to complete one rotation (360°) in the horizontal direction is 100 ms, and 70,000 measurements are obtained in one rotation.

The IMU outputs attitude angles (roll and pitch angles) and their angular velocities every 10 ms. The resolution of attitude angle is $6.0 \times 10^{-3\circ}$ and its error is $\pm 0.5°$ (typ.). The resolution of angular velocity is 0.03 °/s, and its error is ± 0.5 °/s (typ.).

In this paper, one rotation of the lidar beam in the horizontal direction (360°) is referred to as one scan, and the data obtained from this scan is referred to as scan data. The lidar's scan period (100 ms) is denoted as τ and scan-data observation period (0.55 ms) as $\Delta\tau$. The observation period (10 ms) of IMU is denoted as $\Delta\tau_{IMU}$. Therefore, IMU data are obtained 10 times in one scan of the lidar ($\tau = 10\Delta\tau_{IMU}$), and lidar-scan data are obtained 18 times within the observation period of IMU ($\Delta\tau_{IMU} = 18\Delta\tau$).

3 SCAN-DATA MAPPING USING NDT SCAN MATCHING

In the process for scan-data mapping using the NDT scan matching, the scan data captured in the sensor coordinate frame is mapped onto a 3D grid map (a voxel map) represented in the bicycle coordinate frame Σ_b. A voxel grid filter (Munaro et al., 2012) is applied to downsize the scan data. The voxel used for the voxel grid filter is a cube with a side-length of 0.2 m.

In the world coordinate frame Σ_W, a voxel map with a voxel size of 1 m is used for the NDT scan matching. For the i-th ($i = 1, 2, \dots n$) measurement in

the scan data, we define the position vector in Σ_b as $\boldsymbol{p}_{bi}$ and that in Σ_W as $\boldsymbol{p}_i$. Then, the following relationship is given:

$$\begin{pmatrix} \boldsymbol{p}_i \\ 1 \end{pmatrix} = \boldsymbol{T}(\boldsymbol{X}) \begin{pmatrix} \boldsymbol{p}_{bi} \\ 1 \end{pmatrix} \tag{1}$$

where $\boldsymbol{X} = (x, y, z, \phi, \theta, \psi)^T$ is the bicycle's pose. $(x, y, z)^T$ and $(\phi, \theta, \psi)^T$ are the 3D position and attitude angle (roll, pitch, and yaw angles) of the bicycle, respectively, in Σ_W. $\boldsymbol{T}(\boldsymbol{X})$ is the following homogeneous transformation matrix:

$$\boldsymbol{T}(\boldsymbol{X}) = \begin{pmatrix} \cos\theta\cos\psi & \sin\phi\sin\theta\cos\psi - \cos\phi\sin\psi & \cos\phi\sin\theta\cos\psi + \sin\phi\sin\psi & x \\ \cos\theta\sin\psi & \sin\phi\sin\theta\sin\psi + \cos\phi\cos\psi & \cos\phi\sin\theta\sin\psi - \sin\phi\cos\psi & y \\ -\sin\theta & \sin\phi\cos\theta & \cos\phi\cos\theta & z \\ 0 & 0 & 0 & 1 \end{pmatrix}$$

The scan data obtained at the current time $t\tau$ ($t = 0, 1, 2, \ldots$), $\boldsymbol{P}_b(t) = \{\boldsymbol{p}_{b1}(t), \boldsymbol{p}_{b2}(t), \cdots, \boldsymbol{p}_{bn}(t)\}$ or $\boldsymbol{P}(t) = \{\boldsymbol{p}_1(t), \boldsymbol{p}_2(t), \cdots, \boldsymbol{p}_n(t)\}$, are referred to as the new input scan, and the scan data obtained in the previous time before $(t-1)\tau$, $\boldsymbol{P} = \{\boldsymbol{P}(0), \boldsymbol{P}(1), \cdots, \boldsymbol{P}(t-1)\}$, is referred to as the reference scan.

The NDT scan matching (Biber and Strasser, 2003) conducts a normal distribution transformation for the reference scan in each grid on the voxel map; it calculates the mean and covariance of the 3D positions of the lidar-scan data. By matching the new input scan at $t\tau$ with the reference scan obtained prior to $(t-1)\tau$, the bicycle's pose $\boldsymbol{X}(t)$ at $t\tau$ is determined. The bicycle's pose is used for conducting a coordinate transform by Eq. (1), and the new input scan is then mapped to Σ_W.

In this study, we use point cloud library (PCL) for the NDT scan matching (Rusu and Cousin, 2011). It should be noted that the downsized scan data is only used to calculate the bicycle's pose using the NDT scan matching at small computational cost.
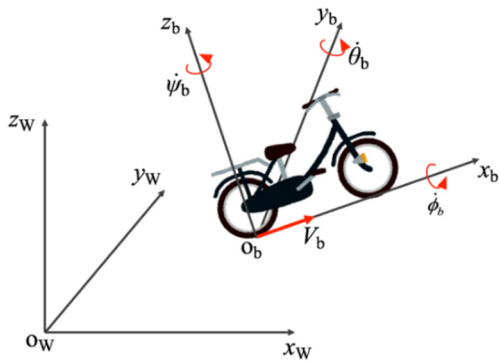
Figure 2: Notation related to bicycle motion.

4 DISTORTION CORRECTION AND MAPPING

4.1 Motion and Measurement Models

As shown in Fig. 2, the linear velocity of the bicycle in Σ_b is denoted as V_b (the velocity in the x_b-axis direction), and the angular velocities about the x_b-, y_b-, and z_b- axes are denoted as $\dot\phi_b$, $\dot\theta_b$, and $\dot\psi_b$, respectively.

If the bicycle is assumed to move at nearly constant linear and angular velocities, the following motion model can be derived (Inui et al., 2017):

$$\begin{pmatrix} x(t+1) \\ y(t+1) \\ z(t+1) \\ \phi(t+1) \\ \theta(t+1) \\ \psi(t+1) \\ V_b(t+1) \\ \dot\phi_b(t+1) \\ \dot\theta_b(t+1) \\ \dot\psi_b(t+1) \end{pmatrix} = \begin{pmatrix} x(t) + a_1(t)\cos\theta(t)\cos\psi(t) \\ y(t) + a_1(t)\cos\theta(t)\sin\psi(t) \\ z(t) - a_1(t)\sin\theta(t) \\ \phi(t) + \{a_2(t)\sin\phi(t) + a_3(t)\cos\phi(t)\}\tan\theta(t) \\ \theta(t) + \{a_2(t)\cos\phi(t) - a_3(t)\sin\phi(t)\} \\ \psi(t) + \{a_2(t)\sin\phi(t) + a_3(t)\cos\phi(t)\}\frac{1}{\cos\theta(t)} \\ V_b(t) + \tau w_{\dot V_b} \\ \dot\phi_b(t) + \tau w_{\ddot\phi_b} \\ \dot\theta_b(t) + \tau w_{\ddot\theta_b} \\ \dot\psi_b(t) + \tau w_{\ddot\psi_b} \end{pmatrix} \tag{2}$$

where $a_1(t) = V_b(t)\tau + \tau^2 w_{\dot V_b}/2$, $a_2(t) = \dot\theta_b(t)\tau + \tau^2 w_{\ddot\theta_b}/2$, and $a_3(t) = \dot\psi_b(t)\tau + \tau^2 w_{\ddot\psi_b}/2$. $w_{\dot V_b}$, $w_{\ddot\phi_b}$, $w_{\ddot\theta_b}$, and $w_{\ddot\psi_b}$ are the acceleration disturbances.

We express Eq. (2) in the following vector form:

$$\boldsymbol{\xi}(t+1) = \boldsymbol{f}\left[\boldsymbol{\xi}(t), \boldsymbol{w}, \tau\right] \tag{3}$$

where $\boldsymbol{\xi} = (x, y, z, \phi, \theta, \psi, V_b, \dot\phi_b, \dot\theta_b, \dot\psi_b)^T$ and $\boldsymbol{w} = (w_{\dot V_b}, w_{\ddot\phi_b}, w_{\ddot\theta_b}, w_{\ddot\psi_b})^T$.

The attitude angle and angular velocity of the bicycle obtained at time $t\tau_{IMU}$ by IMU is denoted as $z_{IMU}(t)$. The measurement model is then

$$\boldsymbol{z}_{IMU}(t) = \boldsymbol{H}_{IMU}\boldsymbol{\xi}(t) + \Delta \boldsymbol{z}_{IMU}(t) \tag{4}$$

where Δz_{IMU} is sensor noise, and $\boldsymbol{H}_{IMU}$ is a measurement matrix.

We also denote the bicycle's pose obtained at $t\tau$ using the NDT scan matching as $\boldsymbol{z}_{NDT}(t) \equiv \hat{\boldsymbol{X}}(t)$. The measurement model is then

$$\boldsymbol{z}_{NDT}(t) = \boldsymbol{H}_{NDT}\boldsymbol{\xi}(t) + \Delta \boldsymbol{z}_{NDT}(t) \tag{5}$$

where Δz_{NDT} is the measurement noise, and $\boldsymbol{H}_{NDT}$ is the measurement matrix.

4.2 Distortion Correction

Figure 3 shows the sequence for correcting distortion in the lidar-scan data. When at the time $(t-1)\tau + (k-1)\Delta\tau_{IMU}$, where k =1–10, the state estimate of the bicycle, $\hat{\xi}^{(k-1)}(t-1)$, and its associated error covariance $\Gamma^{(k-1)}(t-1)$ are obtained, the EKF prediction algorithm (Yaakov et al., 2001) gives the state prediction $\hat{\xi}^{(k/k-1)}(t-1)$ and its error covariance $\Gamma^{(k/k-1)}(t-1)$ at the time $(t-1)\tau + k\Delta\tau_{IMU}$ by

$$\left.\begin{aligned}\hat{\xi}^{(k/k-1)}(t-1) &= f[\hat{\xi}^{(k-1)}(t-1), 0, \Delta\tau_{IMU}] \\ \Gamma^{(k/k-1)}(t-1) &= F(t-1)\Gamma^{(k-1)}(t-1)F(t-1)^T \\ &\quad + G(t-1)QG(t-1)^T\end{aligned}\right\} \quad (6)$$

where $F = \partial f / \partial \hat{\xi}$, $G = \partial f / \partial w$, and Q is the covariance matrix of the plant noise, w.

At the time $(t-1)\tau + k\Delta\tau_{IMU}$, we observe the attitude angle and angular velocity z_{IMU} of the bicycle with IMU. The EKF estimation algorithm (Yaakov et al., 2001) then gives a state estimate $\hat{\xi}^{(k)}(t-1)$ and its error covariance $\Gamma^{(k)}(t-1)$ as follows:

$$\left.\begin{aligned}\hat{\xi}^{(k)}(t-1) &= \hat{\xi}^{(k/k-1)}(t-1) + K\{z_{IMU} \\ &\quad - H_{IMU}\hat{\xi}^{(k/k-1)}(t-1)\} \\ \Gamma^{(k)}(t-1) &= \Gamma^{(k/k-1)}(t-1) \\ &\quad - KH_{IMU}\Gamma^{(k/k-1)}(t-1)\end{aligned}\right\} \quad (7)$$

where $K = \Gamma^{(k/k-1)}(t-1)H_{IMU}^T S^{-1}(t-1)$ and $S = H_{IMU}\Gamma^{(k/k-1)}(t-1)H_{IMU}^T - R_{IMU}$. R_{IMU} is the covariance matrix of the sensor noise Δz_{IMU}.

We denote the state estimate related to the bicycle's pose $(x, y, z, \phi, \theta, \psi)$ as $\hat{X}^{(k)}(t-1) \in \hat{\xi}^{(k)}(t-1)$. Using the state estimates $\hat{X}^{(k-1)}(t-1)$ and $\hat{X}^{(k)}(t-1)$ at the time $(t-1)\tau + (k-1)\Delta\tau_{IMU}$ and $(t-1)\tau + k\Delta\tau_{IMU}$, respectively, the pose $\hat{X}^{(k-1)}(t-1, j)$ of the bicycle at the time $(t-1)\tau + (k-1)\Delta\tau_{IMU} + j\Delta\tau$, where $j = 1$–17, is interpolated by

$$\hat{X}^{(k-1)}(t-1, j) = \hat{X}^{(k-1)}(t-1) \\ + \frac{\hat{X}^{(k)}(t-1) - \hat{X}^{(k-1)}(t-1)}{\Delta\tau_{IMU}} j\Delta\tau \quad (8)$$

Then, the scan data $p_{bi}^{(k-1)}(t-1, j)$ obtained at the time $(t-1)\tau + (k-1)\Delta\tau_{IMU} + j\Delta\tau$ is transformed to $p_i^{(k-1)}(t-1, j)$ as follows:

$$\begin{pmatrix} p_i^{(k-1)}(t-1, j) \\ 1 \end{pmatrix} = T(\hat{X}^{(k-1)}(t-1, j)) \begin{pmatrix} p_{bi}^{(k-1)}(t-1, j) \\ 1 \end{pmatrix} \quad (9)$$
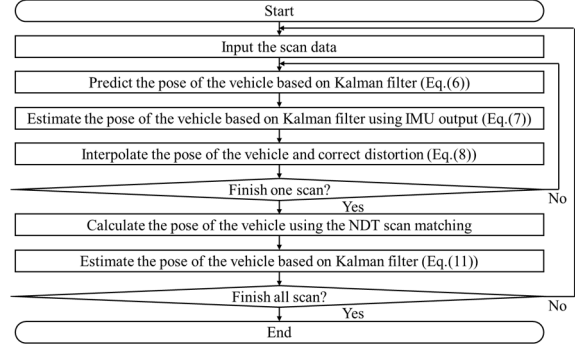
Figure 3: Sequence of correcting distortion in the scan data.

Using the pose estimate $\hat{X}^{(10)}(t-1)$ of the bicycle, the scan data $p_i^{(k-1)}(t-1, j)$ are again transformed to the scan data $P_{bi}^*(t)$ in Σ_b at the time $t\tau$ by

$$\begin{pmatrix} p_{bi}^*(t) \\ 1 \end{pmatrix} = T(\hat{X}^{(10)}(t-1))^{-1} \begin{pmatrix} p_i^{(k-1)}(t-1, j) \\ 1 \end{pmatrix} \quad (10)$$

The scan data corrected with Eq. (10), $P_b^*(t) = \{ p_{b1}^*(t), p_{b2}^*(t), \cdots, p_{bn}^*(t) \}$, are used as the new input scan for scan matching, and the pose angle z_{NDT} of the bicycle at the time $t\tau$ is calculated. In this scan matching, we use the estimate $\hat{X}^{(10)}(t-1)$ as the initial pose in the recursive calculation. Then, the EKF estimation algorithm calculates the state estimate $\hat{\xi}(t)$ and its error covariance $\Gamma(t)$ of the bicycle at the time $t\tau$ as follows:

$$\left.\begin{aligned}\hat{\xi}(t) &= \hat{\xi}^{(10)}(t-1) + K(t)\{z_{NDT}(t) - H_{NDT}\hat{\xi}^{(10)}(t-1)\} \\ \Gamma(t) &= \Gamma^{(10)}(t-1) - K(t)H_{NDT}\Gamma^{(10)}(t-1)\end{aligned}\right\} \quad (11)$$

where, $K(t) = \Gamma^{(10)}(t-1)H_{NDT}^T S^{-1}(t)$, $S(t) = H_{NDT}\Gamma^{(10)}(t-1)H_{NDT}^T - R_{NDT}$, and R_{NDT} is the covariance matrix of Δz_{NDT} .

4.3 Map Generation

We generate the map using the scan data corrected in the previous section.

When the state estimate $\hat{\xi}(t-1)$ and its error covariance $\Gamma(t-1)$ of the bicycle are obtained at the time $(t-1)\tau$, the EKF prediction algoritm obtains the state prediction $\hat{\xi}(t/t-1)$ and its error covariance $\Gamma(t/t-1)$ at the time $t\tau$ as follows:

$$\hat{\xi}(t/t-1) = f[\hat{\xi}(t-1), 0, \tau]$$
$$\Gamma(t/t-1) = F(t-1)\Gamma(t-1)F(t-1)^T$$
$$+ G(t-1)QG(t-1)^T \qquad (12)$$

Here, we denote the state prediction related to the bicycle's pose $(x, y, z, \phi, \theta, \psi)$ as $\hat{X}_{(t/t-1)} \in \hat{\xi}(t/t-1)$.

We use the corrected scan data $P_b^*{}_{(t)} = \left\{ p_{b1}^*{}_{(t)}, p_{b2}^*{}_{(t)}, \cdots, p_{bn}^*{}_{(t)} \right\}$ as the new input scan to perform scan matching. Then, we calculate the pose z_{NDT} of the bicycle at the time $t\tau$. In this scan matching, we use the prediction, $\hat{X}_{(t/t-1)}$ as the initial pose in the recursive calculation.

The new input scan $P_b^*{}_{(t)}$ is mapped on the world coordinate frame Σ_W using $T(z_{NDT})$ in Eq. (1). Then, the EKF estimation algorithm calculates the state estimate $\hat{\xi}_{(t)}$ and its error covariance $\Gamma_{(t)}$ at the time $t\tau$ as follows:

$$\hat{\xi}(t) = \hat{\xi}(t/t-1) + K(t)\{z_{NDT}(t) - H_{NDT}\hat{\xi}(t/t-1)\}$$
$$\Gamma(t) = \Gamma(t/t-1) - K(t)H_{NDT}\Gamma(t/t-1) \qquad (13)$$

where $K_{(t)} = \Gamma_{(t/t-1)}H_{NDT}^T S^{-1}{}_{(t)}$ and

$S_{(t)} = H_{NDT}\Gamma_{(t/t-1)}H_{NDT}^T - R_{NDT}$.

5 EXPERIMENTAL RESULTS

The bicycle moved on a road shown in Fig. 4, and lidar-scan data in 1500 scans (150 seconds) were captured. The maximum velocity of the bicycle was 18 km/h. Figure 5 shows IMU output of roll and pitch angles of the bicycle. To change the attitude of the lidar largely, the bicycle was moved in zigzag. Then, the large rolling motions of the bicycle occurred as shown in Fig. 5 (a).

We evaluate mapping performance in the following four cases:

Case 1: Mapping by the proposed method
Case 2: Mapping without distortion correction
Case 3: Mapping by our previous method (Inui et. al., 2017)
Case 4: Mapping using lidar-scan data, in which distortion is corrected using pose information from onboard GNSS/ IMU unit

In case 3, we correct distortion in the lidar-scan data using only the lidar information (using no IMU information); a bicycle identifies its own 3D pose in a lidar-scan period (0.1 s) using the NDT scan matching. Based on the pose information, the bicycle's pose is estimated every 0.55 ms using the EKF, in which Eqs. (3) and (5) are used as motion and

measurement models, respectively. We then corrected the lidar-scan distortion by the estimated pose.

The bicycle is equipped with the GNSS/IMU unit (Novatel, PwrPak7-E1) to evaluate the bicycle motion in experiments. The root mean square error (RMSE) in horizontal and vertical positions of the GNSS/IMU unit are 0.02 m and 0.03 m, respectively. The RMSE in role/pitch and yaw angles are 0.03° and 0.1°, respectively. In case 4, we measure the bicycle's pose every 0.1s with the GNSS/IMU unit and estimate the bicycle's pose every 0.55 ms using the interpolation method. We then correct the lidar-scan distortion by the interpolated pose.

Figure 6 (a) shows the close-up view of yellow rectangular area shown in Fig. 4. Figure 7 shows the mapping result of the environment in Fig. 6 (a). Figure 8 also shows the mapping result of the traffic sign in Fig. 6(b) and neighbouring tree.

Figure 4: Experimental environment (bird-eye view).
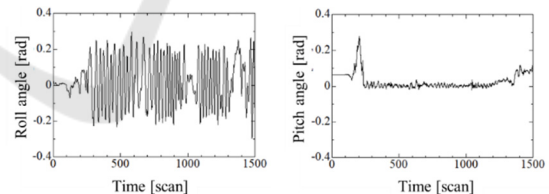
(a) Roll angle.   (b) Pitch angle.

Figure 5: Attitude angle of bicycle.

(a) Mapping environment.   (b) Traffic sign.

Figure 6: Mapping environment and traffic sign.

(a) Case 1 (using proposed method).

(b) Case 2 (without distortion correction).

(c) Case 3 (using previous method).

(d) Case 4 (using distortion correction by pose information from GNSS/IMU unit).
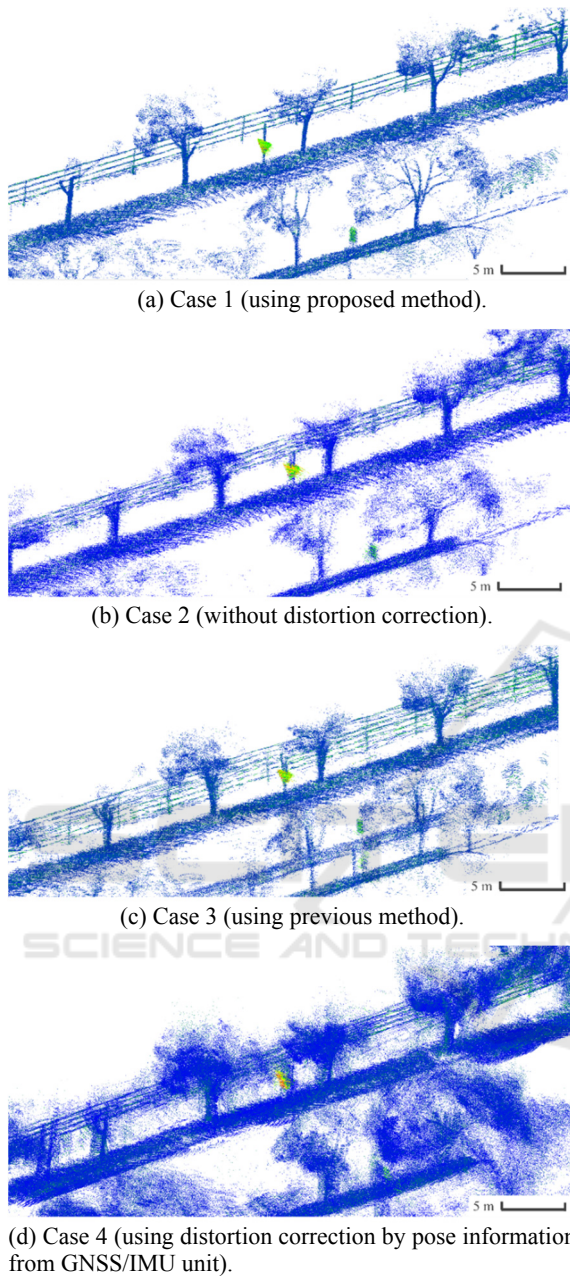
Figure 7: Result of environment mapping. Different coloured dots indicate lidar-scan data with different reflective intensities.

It is clear from Figs. 7 and 8 that the mapping result by the proposed method (case 1) is more crispness than that by the other methods.

(a) Case 1.

(b) Case 2.

(c) Case 3.

(d) Case 4.
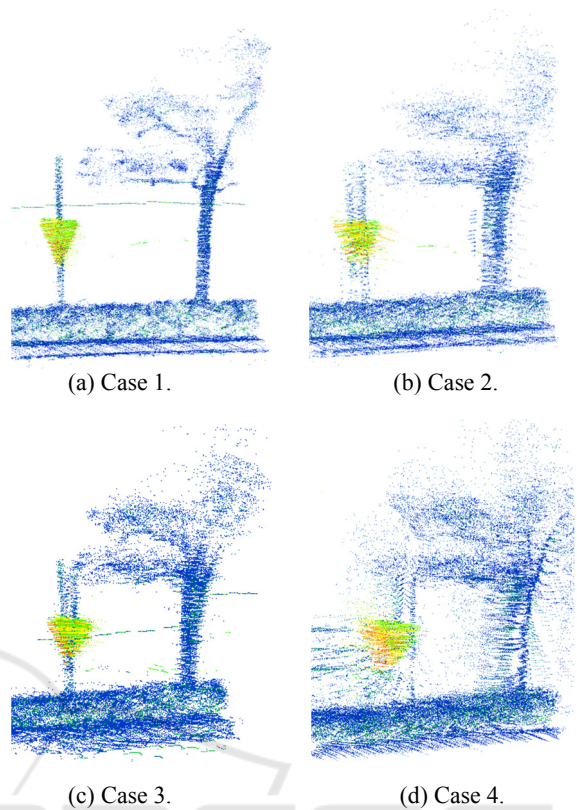
Figure 8: Mapping result of traffic sign and tree.

6 CONCLUSIONS

In this paper, we proposed a method to generate 3D point-cloud maps with a lidar mounted on a two-wheeled vehicle. Distortion in lidar-scan data that occur by sudden changes of the vehicle's pose were corrected; pose of the two-wheeled vehicle were calculated by the NDT scan matching using the lidar-scan data obtained at each scan period.

The distortion in the scan data was corrected by estimating the vehicle's pose in a period shorter than the scan period via the EKF and interpolation method using the information of the NDT scan matching and IMU. The corrected scan data were applied to accurate 3D point-cloud mapping.

The experimental results of road-environment mapping by a 32-layer lidar mounted on a bicycle validated the efficacy of the proposed method.

As future works, we will perform reduction in computational costs in mapping, quantitative evaluation of the mapping performance, and experiments using a lidar mounted on a motorcycle.

ACKNOWLEDGEMENTS

REFERENCES

Biber, P., and Strasser, W., 2003, The Normal Distributions Transform: A New Approach to Laser Scan Matching, In *Proceedings of IEEE/RSJ International Conference on Intelligent Robots and Systems* (*IROS 2003*), pp. 2743–2748.

Bosse, M., Zlot, R. and Flick, P., Zebedee, 2012, Design of a Spring-Mounted 3-D Range Sensor with Application to Mobile Mapping, In *IEEE Transactions on Robotics*, Vol. 28, Issue 5, pp. 1104–1119.

Brenneke, C., Wulf, O., and Wagner, B., 2003, Using 3D Laser Range Data for SLAM in Outdoor Environments, In *Proceedings of IEEE/RSJ International Conference on Intelligent Robots and Systems* (*IROS 2003*), pp. 188–193.

Cadena, C., Carlone, L., and Carrillo, H., et al., 2016, Past, Present, and Future of Simultaneous Localization and Mapping: towards the Robust-perception Age, In *IEEE Transactions on Robotics*, Vol. 32, No. 6, pp 1309–1332.

Hong, S., Ko, H. and Kim, J., 2010, VICP: Velocity Updating Iterative Closest Point Algorithm, In *Proceedings of 2010 IEEE International Conference on Robotics and Automation* (*ICRA 2010*), pp. 1893–1898.

Inui, K., Morikawa, M., Hashimoto, M., Tokorodani, K. and Takahashi, K., 2017, Distortion Correction of Laser Scan Data from In-vehicle Laser Scanner based on NDT scan-matching, In *Proceedings of the 14th International Conference on Informatics in Control, Automation and Robotics* (*ICINCO* 2017), pp. 329–334.

Kawahara, T., Ohno, K. and Tadokoro, S., 2006, Localization and Mapping for Fast Mobile Robots with 2D Laser Range Finder, *In Proceedings of the 2006 JSME Conference on Robotics and Mechatronics* (in Japanese).

Kuramachi, R., Ohsaro, A., Sasaki, Y. and Mizoguchi, H., 2015, G-ICP SLAM: An Odometer-free 3D Mapping System with Robust 6dof Pose Estimation, In *Proceedings of the 2015 IEEE Conference on Robotics and Biomimetics* (*ROBIO* 2015), pp. 176–181.

Moosmann, F. and Stiller, C., 2011, Velodyne SLAM, In *Proceedings of IEEE Intelligent Vehicles Symposium* (*IV2011*), pp. 393–398.

Morita, K., Hashimoto, M., and Takahashi, K., 2019, Point-Cloud Mapping and Merging using Mobile Laser Scanner, In *Proceedings of the Third IEEE International Conference on Robotic Computing* (*IRC 2019*), pp.417–418.

Munaro, M., Basso, F., and Menegatti, E., 2012, Tracking People within Groups with RGB-D Data, In *Proceedings of IEEE/RSJ International Conference on Intelligent Robots and Systems* (*IROS* 2012), pp. 2101–2107.

Rusu, R. B., and Cousins, S., 2011, 3D is here: Point Cloud Library (PCL), In *Proceedings of 2011 IEEE International Conference on Robotics and Automation* (*ICRA* 2011).

Seif, H. G., and Hu, X., 2016, Autonomous Driving in the iCity—HD Maps as a Key Challenge of the Automotive Industry, In *Engineering*, Vol. 2, pp.159–162.

Schwesinger, D., Shariati, A., Montella, C., and Spletzer, J., 2017, A Smart Wheelchair Ecosystem for Autonomous Navigation in Urban Environments, In *Autonomous Robot,* Vol. 41, pp. 519–538.

Wang, L., Zhang, Y., and Wang, J., 2017, Map-Based Localization Method for Autonomous Vehicles Using 3D-LIDAR, In *IFAC-Papers OnLine*, Vol. 50, Issue 1, pp. 276-281.

Yaakov, B., Li, X. and Kirubarajan, T., 2001, Estimation with Applications to Tracking and Navigation, John Wiley & Sons, Inc.

Zhang, J. and Singh, A., 2014, LOAM: Lidar Odometry and Mapping in Real-time, In *Proceedings of Robotics: Science and Systems*.